LIMNOLOGY and OCEANOGRAPHY

ASLO

Limnol. Oceanogr. 68, 2023, 1880–1894

doi: 10.1002/lno.12392

Physiological response of an Antarctic cryptophyte to increasing temperature, CO_2, and irradiance

Marianne G. Camoying ,* **Scarlett Trimborn**
Ecological Chemistry, Alfred Wegener Institute, Helmholtz Centre for Polar and Marine Research, Bremerhaven, Germany

Abstract

The Southern Ocean, a globally important CO_2 sink, is one of the most susceptible regions in the world to climate change. Phytoplankton of the coastal shelf waters around the Western Antarctic Peninsula have been experiencing rapid warming over the past decades and current ongoing climatic changes will expose them to ocean acidification and high light intensities due to increasing stratification. We conducted a multiple-stressor experiment to evaluate the response of the still poorly studied key Antarctic cryptophyte species *Geminigera cryophila* to warming in combination with ocean acidification and high irradiance. Based on the thermal growth response of *G. cryophila*, we grew the cryptophyte at suboptimal (2°C) and optimal (4°C) temperatures in combination with two light intensities (medium light: 100 μmol photons m^{-2} s^{-1} and high light [HL]: 500 μmol photons m^{-2} s^{-1}) under ambient (400 μatm pCO_2) and high pCO_2 (1000 μatm pCO_2) conditions. Our results reveal that *G. cryophila* was not susceptible to high pCO_2, but was strongly affected by HL at 2°C, as both growth and carbon fixation were significantly reduced. In comparison, warming up to 4°C stimulated the growth of the cryptophyte and even alleviated the previously observed negative effects of HL at 2°C. When grown, however, at temperatures above 4°C, the cryptophyte already reached its maximal thermal limit at 8°C, pointing out its vulnerability toward even higher temperatures. Hence, our results clearly indicate that warming and high light and not pCO_2 control the growth of *G. cryophila*.

The Southern Ocean is reported to have stored not only large quantities of atmospheric carbon dioxide (CO_2) but also a significant amount of heat associated with climate change (Frölicher et al. 2015). The coastal waters of the Western Antarctic Peninsula (WAP), for example, has been experiencing rapid warming for the past several decades (Jones et al. 2019). Climate model projections show that the Southern Ocean would experience between a ~2°C up to ~6°C increase in temperature by 2100 and 2300, respectively (Boyd et al. 2015; Moore et al. 2018; IPCC 2019). In fact, an unprecedented mean temperature anomaly of +4.5°C has just been reported in the WAP coastal waters in February 2020 (González-Herrero et al. 2022). In this region, previous warming events have been associated with the increasing dominance of cryptophytes over diatoms under conditions of lowered salinity due to the increased sea ice retreat and glacial melting as a result of warming (Mendes et al. 2013; Schofield et al. 2017). As cryptophytes are not the preferred food of krill, the increasing dominance of cryptophytes over diatoms would potentially also alter the Antarctic marine food web (Meyer and El-Sayed 1983). The shift from diatoms to cryptophytes could also result in a reduced drawdown of atmospheric CO_2 in the WAP (Brown et al. 2019). Coastal shelf phytoplankton communities along the WAP are also projected to be more prone to high light exposure due to warming and the subsequently increased freshwater input from the sea-ice melt. The latter potentially enhances vertical stratification and thus results in shoaling of the mixed layer depth and thus more illuminated surface waters (Boyd et al. 2015). At present, studies looking at the effects of high irradiances on Antarctic phytoplankton are still scarce. In addition, due to anthropogenic emissions, the present-day CO_2 level of 413 ppm is going to increase at an unprecedented rate (Hoegh-Guldberg and Bruno 2010) and is projected to reach 936 ppm by 2100 (IPCC 2014). The implications of increased pCO_2 levels in particular on Antarctic cryptophytes is only poorly understood, with the few studies available pointing toward a high pCO_2 tolerance of this group

*Correspondence: marianne.camoying@awi.de

Additional Supporting Information may be found in the online version of this article.

Author Contribution Statement: M.C. and S.T. designed the research. M.C. performed the research and analyzed the data. M.C. and S.T. interpreted the data and wrote the manuscript.

(Schulz et al. 2017; Donahue et al. 2019). Overall, studies looking at the effects of future climate change scenarios such as warming, ocean acidification, and high light on Antarctic cryptophytes are at present still lacking.

Along the WAP, the cryptophyte *Geminigera* is the most abundant genus observed in coastal shelf waters (Brown et al. 2021). In response to warming, laboratory experiments have shown that the Antarctic *Geminigera cryophila* exhibited enhanced growth up to the highest temperature treatment of 4°C (Wang and Smith 2021). Whether the cryptophyte would be able to outcompete other phytoplankton groups at much higher temperatures still yet remains unknown. In response to high irradiances (500 μmol photons m^{-2} s^{-1}), *G. cryophila* was strongly negatively impacted (Trimborn et al. 2019). The reasons for this are not yet clear. On the other hand, it was reported that *G. cryophila* was not negatively affected by high pCO_2 (Trimborn et al. 2019; Camoying et al. 2022), similar to what has been observed for cryptophytes in general when natural phytoplankton were grown under elevated pCO_2 levels (Sommer et al. 2015; Schulz et al. 2017; Donahue et al. 2019). This is in line with the findings that cryptophytes are able to grow within a broad pH range (i.e., at both lower and upper extreme of the pH spectrum, Weisse and Stadler 2006; Gaillard et al. 2020).

As *G. cryophila* represents an important and abundant species in coastal shelf waters along the WAP (Brown et al. 2021), we investigated the combined effects of warming, ocean acidification (high pCO_2) and high light on its physiology. It still remains unexplored how all three environmental factors will influence the ecophysiology of the cryptophyte. Hence, it was the objective of our study to (1) characterize its thermal performance and to (2) identify its physiological strategies to cope with future climate change conditions such as warming in conjunction with high pCO_2 and increasing light.

Methods

Experimental design and culture conditions

We examined the interactive effects of increasing pCO_2, temperature and light on growth, carbon fixation, and photophysiology of the Antarctic cryptophyte *G. cryophila* (CCMP 2564, isolated from McMurdo Sound, Ross Sea, Antarctica). All *G. cryophila* cells grew at 2°C and 100 μmol photons m^{-2} s^{-1} under a 16 : 8 h light–dark cycle. The species was grown in sterile-filtered (0.2 μm) unbuffered natural Antarctic seawater, which was enriched with macronutrients (100 μmol L^{-1} NO_3^- and 6.25 μmol L^{-1} PO_4^{-3}), vitamins (30 nmol L^{-1} B_1, 23 nmol L^{-1} B_7, and 0.228 nmol L^{-1} B_{12}) and trace metals according to $F/2_R$ medium (Guillard and Ryther 1962). Nitrate and phosphate were added following the Redfield N : P ratio of 16 : 1 (Redfield 1958).

To determine the thermal functional response curve of *G. cryophila*, experiments were done at 100 μmol photons m^{-2} s^{-1} under a 16 : 8 light–dark cycle and 400 μatm pCO_2 (bubbled). All *G. cryophila* cultures were grown in triplicate 1 L custom-made cylindrical glass bottles under a range of temperatures, starting at 2°C and then gradually transferred to 4°C, 6°C, 7°C, and 8°C (Fig. 1). More specifically, we followed the methods of Zhu et al. (2017) and did a series of step-wise transfers, making sure that *G. cryophila* cultures were well-acclimated to the lower temperature before exposing them to a higher temperature (Fig. 1). Please note that at 8°C *G. cryophila* died.

For the main temperature-CO_2-light experiment, we chose the temperature treatments based on the outcome of the experiment on the thermal functional response curve of *G. cryophila* (Fig. 2). As 4°C was identified to be the optimal growth of this species based on Fig. 2, we wanted to investigate the response of *G. cryophila* under suboptimal (2°C), optimal (4°C), and supraoptimal (6°C) temperatures (Fig. 1).

Next to the different temperature conditions, *G. cryophila* cells were further grown under two light intensities (*medium light treatment*: 100 μmol photons m^{-2} s^{-1}; *high light treatment*: 500 μmol photons m^{-2} s^{-1}) in combination with two pCO_2 levels (*400 treatment*: 400 μatm pCO_2; *1000 treatment*: 1000 μatm pCO_2). The light intensities of the medium light treatment chosen mimic realistic average daily irradiances of surface coastal waters of the WAP (~ 100 up to 570 μmol photons m^{-2} s^{-1}; Young et al. 2015*a*; Heiden et al. 2019) while the elevated mean irradiance of the high light treatment simulates future light conditions. Moreover, *G. cryophila* was also grown under pCO_2 levels representing values of present-day (~ 410 ppm), and those projected for the year 2100 (~ 1000 μatm, RCP8.5 scenario; IPCC 2014). The two different pCO_2 levels were achieved by gentle bubbling of each culture bottle with humidified air of the respective pCO_2 level. To this end, a mixture of CO_2-free air (< 1 ppmv CO_2; Dominic Hunter) and pure CO_2 (Air Liquide Deutschland Ltd.) was used and controlled through a gas flow controller (CGM 2000; MCZ Umwelttechnik) to generate the two target pCO_2 treatments. A non-dispersive infrared analyzer system (LI6252; Li-Cor Biosciences), which was calibrated with CO_2-free air and purchased gas mixtures of 150 ± 10 and 1000 ± 20 ppmv CO_2 (Air Liquide, Deutschland), was utilized regularly to monitor the different CO_2 gas mixtures. Light-emitting diodes (LED) lamps (SolarStinger LED SunStrip Marine Daylight, Econlux) were used as light source and light intensities were set and monitored using an LI-1400 data logger (Li-Cor) with a 4π-sensor (Walz). Water temperature of the aquaria was also regularly checked to make sure that the cultures were grown under stable temperature.

Prior to the start of the main experiment, cultures were pre-acclimated to each temperature-light-pCO_2 treatment for at least 15 d. During both the preacclimation period and the main experiment, cultures were diluted semi-continuously (before cell density reached 15,000 cells mL^{-1}) with preconditioned media to keep cells in exponential growth, thus ensuring that cells were in the same physiological state

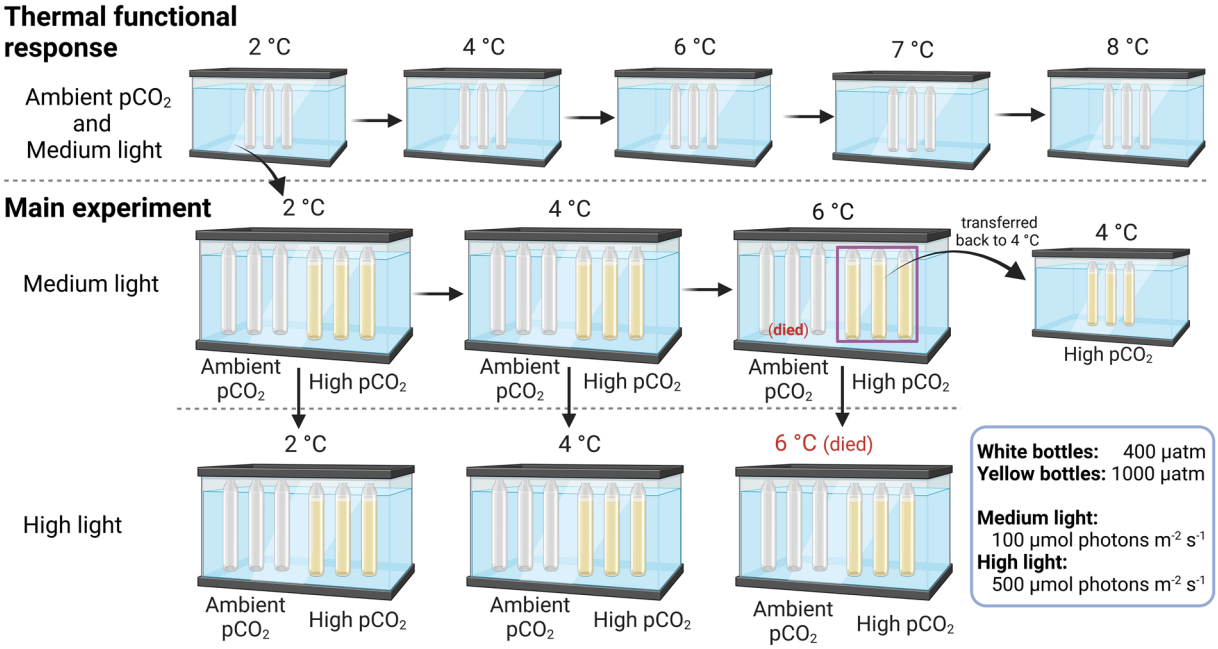

Fig. 1. Overview of the experimental setup (illustration created with BioRender.com). To determine the thermal response curve of *Geminigera cryophila*, cultures were grown at the medium light (ML) intensity of 100 μmol photons m^{-2} s^{-1} and at the ambient pCO_2 of 400 μatm in triplicate 1 L custom-made cylindrical glass bottles under a range of temperatures, starting at 2°C and then gradually transferred to 4°C, 6°C, 7°C, and 8°C. At 8°C *G. cryophila* died. Based on the thermal response, for the main experiment *G. cryophila* was grown at 2°C, 4°C, and 6°C. Each temperature treatment was then combined with two pCO_2 levels (white color: ambient pCO_2 of 400 μatm; yellow: high pCO_2 of 1000 μatm) and two light intensities (medium light and high light). Except for the 6°C-1000-ML treatment, all other 6°C treatments died. To test whether the 6°C-1000-ML treatment could recover from warming stress, it was transferred back to 4°C.

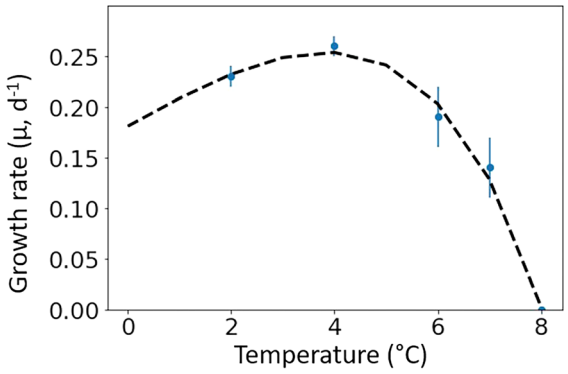

Fig. 2. Thermal functional response curve showing the specific growth rates (μ) of *Geminigera cryophila* at 400 μatm pCO_2 and 100 μmol photons m^{-2} s^{-1} across a range of temperatures from 2°C to 8°C. Values represent the mean and standard deviation ($n = 3$).

during sampling. The starting cell density of cultures in the main experiment was ca. 1000 cells mL^{-1} and final sampling was conducted when densities reached ca. 15,000–20,000 cells mL^{-1}, this ensured a stable carbonate chemistry over the whole experimental time (Table 1).

Due to the small volume of the incubation bottles (ca. 1 L), dilutions were done and final sampling were conducted in batches. This was to make sure that we have enough biomass for each parameter and cell densities are not too high, thus avoiding a shift in the carbonate chemistry as well as potential cell self-shading. In total, the main experiment lasted ca. 10–20 d depending on the treatments. Please note that apart from the medium light-high pCO_2 treatment, in all other 6°C treatments *G. cryophila* was not able to maintain exponential growth and stopped growing after ca. 4 weeks (Fig. 3). To test whether the 6°C-1000-medium light treatment of *G. cryophila* would be able to recover from warming, after 11 weeks of incubation we transferred the 6°C-1000-medium light treatment back to 4°C (ca. 2 weeks preacclimation and 1 week in main experiment) (Fig. 1). From this treatment, we collected triplicate samples for particulate organic carbon (POC), pigments, and conducted chlorophyll *a* (Chl *a*) fluorescence measurements, as will be described later. Hence, the main experiment includes 2°C and 4°C treatments and findings from the 6°C-high pCO_2-medium light treatment.

Carbonate chemistry

To ensure that there would be no pH drift (≤ 0.06 pH units) in cultures, the pH (NBS) was measured regularly in all incubation and culture medium bottles over the duration of the whole experiment (Table 1). Measurements were done with a pH meter (826 pH mobile; Metrohm), which was calibrated (3-point calibration) prior to usage with the National Institute of Standards and Technology-certified buffer systems. At the

Table 1. The CO2Sys program (Pierrot et al. 2006) was used to calculate the dissolved inorganic carbon (DIC) concentrations and the partial pressure of CO_2 (pCO_2) from the measured total alkalinity (TA), pH, silicate, phosphate, salinity, and temperature sampled at the end of the experiment. Values represent mean and SD of each pCO_2 level for both light (medium light and high light) and temperature (2°C and 4°C) treatments (incubation, $n = 12$; medium, $n = 8$). Significant differences between the two pCO_2 treatments (post hoc tests) are indicated by varying lower case letters in superscript ($p < 0.05$).

	Target pCO_2 (μatm)	Calculated pCO_2 (μatm)	Measured pH (NBS)	Measured TA (μmol kg^{-1})	Calculated DIC (μmol kg^{-1})
Geminigera incubations	400	430 ± 60^{a}	8.09 ± 0.05^{a}	2314 ± 27^{a}	2192 ± 28^{a}
Medium (no cells)	400	429 ± 68^{a}	8.08 ± 0.05^{a}	2294 ± 51^{ab}	2173 ± 56^{a}
Geminigera incubations	1000	1035 ± 99^{b}	7.73 ± 0.04^{b}	2319 ± 22^{a}	2307 ± 27^{b}
Medium (no cells)	1000	1060 ± 66^{b}	7.72 ± 0.03^{b}	2282 ± 8^{b}	2275 ± 14^{b}

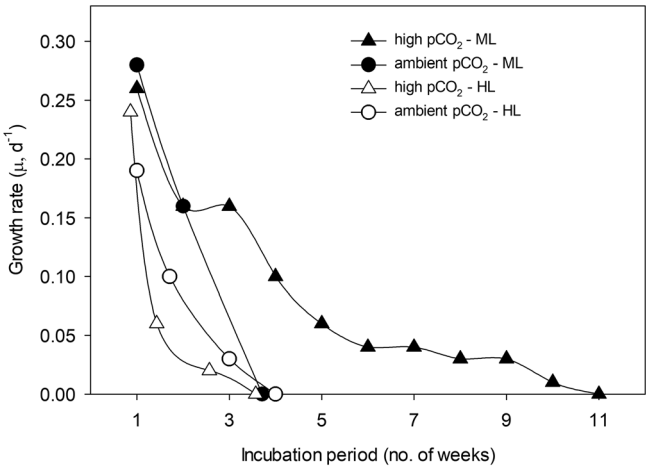

Fig. 3. Growth rates (μ) of *Geminigera cryophila* at 6°C under ambient pCO_2 (400 μatm, filled symbols) and high pCO_2 (1000 μatm, open symbols) in combination with different light intensity (medium light, ML: 100 μmol photons m^{-2} s^{-1}; high light, HL: 500 μmol photons m^{-2} s^{-1}) treatments. All high light treatments and the ambient pCO_2-medium light cultures died after 4 weeks of incubation. Main experiment for the high pCO_2-medium light treatment was aborted as growth stopped.

end of the experiment, samples for total alkalinity (TA) analysis were collected from all incubation and medium bottles by filtering a sample through a glass fiber filter (GF/F; Whatman) and placing the filtrate into 200 mL borosilicate flasks. TA samples were measured in duplicates by potentiometric titrations via a TW alpha plus (SI Analytics). Systematic errors were corrected with certified reference material (from Prof. A Dickson, Scripps, USA; batch no. 161). TA, pH, silicate, phosphate, temperature, and salinity measurements were used to determine the seawater carbonate chemistry using the CO2Sys program (Pierrot et al. 2006), wherein the equilibrium constant of Mehrbach et al. (1973) refitted by Dickson and Millero (1987) was utilized.

Cell density and thermal functional response curve

Cell densities were regularly monitored and samples were taken at the same time of the day at the start, during, and the end of both the thermal functional response experiment and the main experiment. To this end, a Beckman Multisizer 3 Coulter Counter with a 100 μm aperture was used to determine cell density immediately after sampling. Growth rates (μ; d^{-1}) of *G. cryophila* under all experimental treatments were determined and were calculated using the formula:

$$\mu = \frac{\ln\left(\frac{N_t}{N_0}\right)}{t}, \quad (1)$$

where N_t refers to the cell density during the final harvest and N_0 to the one at the start of the experiment. The duration between both sampling points is represented by t. To describe the thermal growth response curve of *G. cryophila*, a modified Ratkowsky equation (Ratkowsky et al. 1983; Zwietering et al. 1991) was used:

$$\mu_{max} = [b(T - T_{min})]^2 \times \left\{1 - e^{[c(T - T_{max})]}\right\} \quad (2)$$

where μ_{max} is the maximum specific growth rate, T_{min} and T_{max} are the minimum and maximum temperatures, respectively, at which the growth rate is zero, while b and c are Ratkowsky parameters that possess no specific biological meaning. The optimum temperature for growth (T_{opt}) was derived from the fitted curve as the temperature at which the growth rate was the highest.

Pigments

At the end of the experiment, pigment samples were collected by filtering the cultures onto GF/F filters (~ 0.6 μm, 25 mm; Whatman) and directly freezing them in liquid nitrogen. After storage at −80°C, the extraction and Chl *a* and chlorophyll c_2 (Chl c_2) analysis was done as described in Camoying et al. (2022). To calculate cellular quotas, Chl *a* and Chl c_2 contents were normalized to filtered volume and cell densities.

POC and particulate organic nitrogen quotas

At the end of the experiment, samples for POC and particulate organic nitrogen (PON) were collected by gently filtering (< 20 mmHg) cultures onto precombusted glass fiber filters

(15 h, 200°C, GF/F, ~ 0.6 μm, 25 mm; Whatman). Filters were then stored at −20°C and were oven-dried first overnight (> 12 h, 60°C) before acidifying them with 200 μL of 0.2 N HCl. The acidified filters were again oven-dried (> 12 h, 60°C) and analyzed on an automated carbon nitrogen elemental analyzer (EURO EA-CN Elemental Analyzer; HEKAtech GmbH). Samples for blank measurements were also prepared. In order to determine cellular quotas, the blank-corrected POC/PON values were normalized with the filtered volume and cell densities. To calculate cellular daily production rates of POC and PON, cellular quotas were multiplied by the corresponding growth rate of the respective treatment. Molar ratios of carbon to nitrogen (C : N) were also calculated.

Photophysiology

A Fast Repetition Rate fluorometer (FastOcean PTX; Chelsea Technologies Group Ltd.) coupled with a FastAct Laboratory system (Chelsea Technologies Group Ltd.) was used to assess the photophysiological response of *G. cryophila* under all pCO_2-temperature-light treatments at the end of the experiment. Prior to the Chl *a* fluorescence measurements, cells were dark-adapted for 10 min at the respective growth temperature to ensure open photosystem II (PSII) reaction centers and no occurrence of non-photochemical quenching. The minimum Chl *a* fluorescence (F_0) was recorded immediately after the dark-acclimation phase. To gradually saturate PSII, a single turnover flashlet of 1.2×10^{22} photons $m^{-2} s^{-1}$ and a wavelength of 450 nm was applied consisting of 100 flashlets on a 2 μs pitch. A relaxation phase of 40 flashlets on a 50 μs pitch was subsequently done. This combination of saturation-relaxation phases was reiterated 6 times for every acquisition. To determine the maximum (F_m) Chl *a* fluorescence, the saturation phase of the single turnover was fitted according to Kolber et al. (1998). The dark-adapted maximum quantum yield of photosynthesis of PSII (F_v/F_m) was then calculated using the equation:

$$F_v/F_m = \frac{(F_m - F_0)}{F_m}. \quad (3)$$

The energy transfer between PSII units (i.e., connectivity, *P*), the functional absorption of PSII photochemistry (σ_{PSII}) and the concentration of functional PSII reaction centers ([RCII]) were also determined from the single turnover measurement of the dark-adapted cells.

Fluorescence light curves were also done, which lasted in total for ca. 1 h. During the fluorescence light curves, cells were exposed to increasing light intensities (30–900 μmol photons $m^{-2} s^{-1}$) for 5 min per light step. After each light intensity, six Chl *a* fluorescence measurements were carried out. The light-adapted minimum (F') and maximum (F_m') Chl *a* fluorescence of the single turnover acquisition were estimated from these measurements. The effective PSII quantum yield under ambient light (F_q'/F_m') was calculated according to the equation $(F_m' - F')/F_m'$ (Genty et al. 1989). The absolute electron transport rates (ETR) were calculated following Suggett et al. (2004, 2009):

$$ETR = \sigma_{PSII} \times \left(\frac{F_{q'}/F_{m'}}{F_v/F_m}\right) \times E, \quad (4)$$

where σ_{PSII} is the functional absorption cross-section of PSII's photochemistry (nm^2) and *E* the instantaneous irradiance (photons $m^{-2} s^{-1}$). Irradiance-dependent ETRs were curve-fitted according to Ralph and Gademann (2005) to determine maximum ETR (ETR_{max}), minimum saturating irradiance (I_k) and maximum light utilization efficiency (α).

Statistical analyses

A three-way ANOVA with Tukey's multiple comparison post hoc tests was done using Graphpad Prism 9 Statistical Software. The independent variables consisted of two temperatures (2°C and 4°C), two light intensities (100 and 500 μmol photons $m^{-2} s^{-1}$) and two pCO_2 levels (400 and 1000 μatm). The interactive effects of the three factors temperature, light, and pCO_2 were examined on all parameters. Graphs were created using SigmaPlot 12.0 (Systat Software, Inc.). All statistical tests were done at the 95% confidence interval. Python 3.8 was used to generate the corresponding thermal response curve by performing curve fitting on the measured growth rates with the modified Ratkowsky equation (using *scipy* curve fit function).

Results

Seawater carbonate chemistry

A stable carbonate chemistry was maintained throughout the course of the experiment (Table 1). For both *G. cryophila* incubations (containing cells) and culture medium (without cells) bottles, pCO_2, pH, and DIC values were significantly different between all ambient pCO_2 and OA treatments ($p < 0.0001$). Among the incubation bottles, TA remained the same irrespective of the applied pCO_2 level (Table 1).

Thermal functional response curve

Growth of *G. cryophila* was strongly influenced by increasing temperature (Fig. 2). Measured growth rate increased from 2°C to 4°C and started to decline at 6°C until growth stopped at 8°C. Based on the thermal response curve of *G. cryophila*, the optimum temperature (T_{opt}) for maximum growth ($\mu_{max} = 0.25$) of the cryptophyte was at 3.80°C. The maximum (T_{max}) temperature, wherein positive growth could still be maintained, was 8.02°C.

Growth, carbon production, and pigment cellular concentration

High pCO_2 did not affect the growth of *G. cryophila* in all treatments (Fig. 4A). In response to increasing temperature up to 4°C, growth was generally significantly enhanced

irrespective of the applied light intensity and pCO_2 level ($p < 0.0001$). Only under medium light and high pCO_2 conditions, increasing temperature did not alter growth. A significant medium light effect ($p < 0.01$) on growth was evident, as growth rates were significantly reduced in the 2°C treatment under each pCO_2 level. At 4°C, growth remained unchanged with increasing irradiance. A significant interactive effect was observed only between temperature and light ($p < 0.05$; Table 2).

For the 6°C-medium light-400 treatment, growth was reduced by 73% after 2 weeks of incubation (Fig. 3; Table 3) relative to the 4°C-medium light-400 treatment (Fig. 4A). After 4 weeks of incubation, the 6°C-400-medium light cells stopped growing. Only under high pCO_2, the medium light treatment grew very slowly at 6°C, and finally stopped growing after 11 weeks (Fig. 3; Table 3). Moreover, the latter exhibited morphological changes typical for unhealthy cells such as compromised cell membrane (i.e., bubble-like formation) and the appearance of hair-like projections (Supporting Information Fig. S1). When the 6°C-medium light-1000 treatment was transferred back to 4°C, it recovered and exhibited growth rates ($\mu = 0.27 \pm 0.01$ d^{-1}; Table 3) comparable to the 4°C-medium light-400 treatment ($\mu = 0.26 \pm 0.01$ d^{-1}; Fig. 4A).

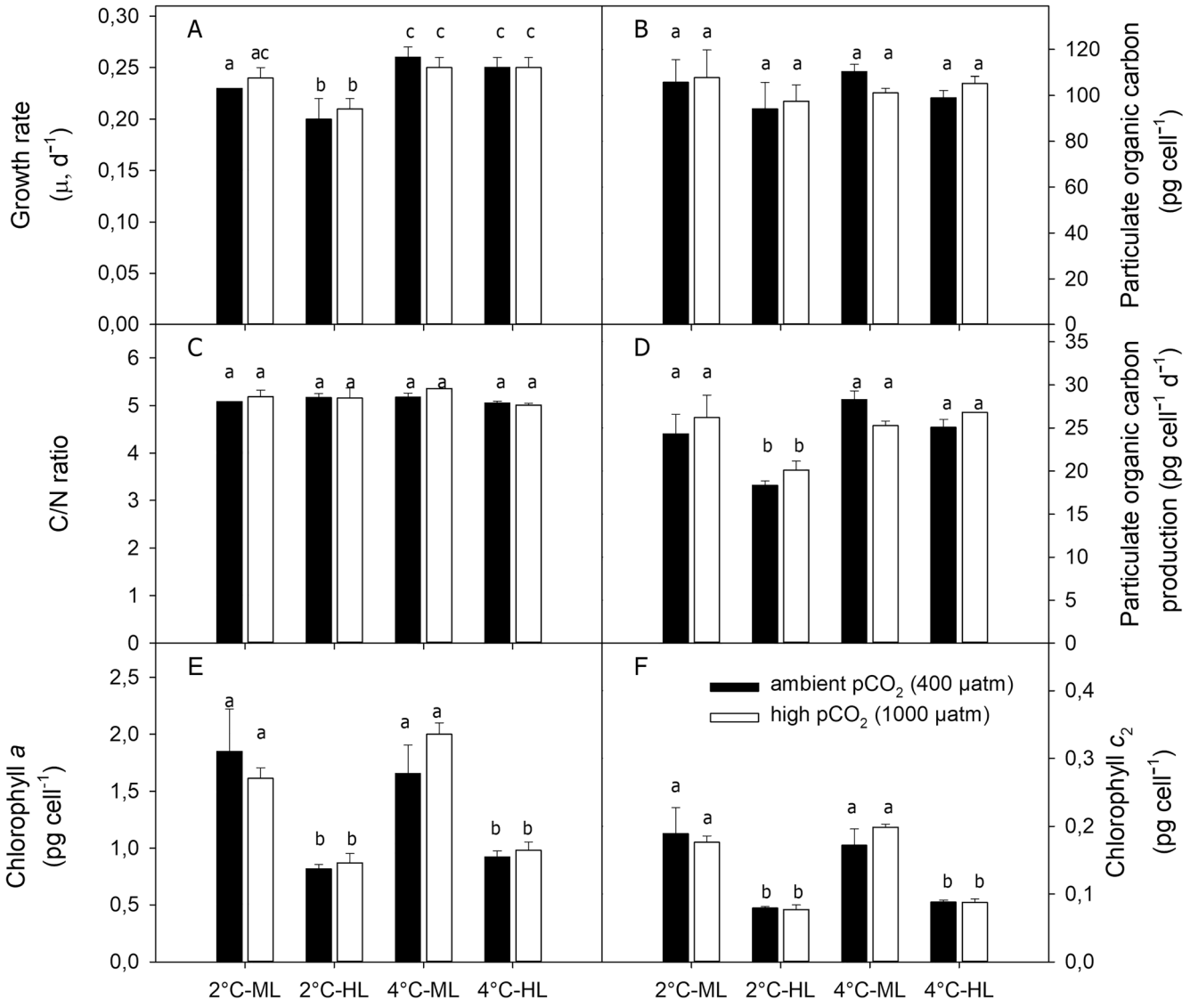

Fig. 4. Growth rates (**A**), cellular particulate organic carbon (POC) contents (**B**), molar carbon to nitrogen (C/N) ratios (**C**), POC production rates (**D**), and cellular concentrations of chlorophyll *a* (**E**) and chlorophyll c_2 (**F**) of *Geminigera cryophila* were determined under ambient pCO_2 (400 μatm, dark bars) and high pCO_2 (1000 μatm, white bars) in combination with different temperature (2°C and 4°C) and light (medium light, ML: 100 μmol photons m^{-2} s^{-1}; high light, HL: 500 μmol photons m^{-2} s^{-1}) treatments at the end of the experiments. Values represent the mean and standard deviation ($n = 3$). Significant differences between the two pCO_2 treatments (post hoc tests) are indicated by varying lower case letters ($p < 0.05$).

Table 2. Significance of interactive effects of pCO_2, light and temperature ($p < 0.05$) on the growth rate (μ), particulate organic carbon (POC) quota and production, C : N ratio, cellular chlorophyll *a* (Chl *a*) and chlorophyll c_2 (Chl c_2) concentrations, as well as the dark-adapted maximum photosystem II quantum yield (photosynthetic yield, F_v/F_m), yield recovery (F_v/F_m recovery), energy transfer between photosystem II units (connectivity, *P*), functional absorption cross-section of PSII (σ_{PSII}), reoxidation times of the primary electron acceptor Q_a (τ_{Qa}), cellular concentration of functional PSII reaction centers ([RCII]), maximum electron transport rates (ETR_{max}), minimum saturating irradiance (I_k), and the maximum light utilization efficiency (α) of *Geminigera cryophila*. Statistically insignificant effects ($p > 0.05$) are denoted by n.s.

Parameters	pCO_2	Light	Temperature	Temperature and light	Temperature and pCO_2	Light and pCO_2	Temperature, light, and pCO_2
Growth	n.s.	<0.05	<0.0001	<0.05	n.s.	n.s.	n.s.
POC content	n.s.	n.s.	n.s.	n.s.	n.s.	n.s.	n.s.
POC production	n.s.	0.0001	<0.0001	<0.05	n.s.	n.s.	n.s.
C : N	n.s.	n.s.	n.s	<0.05	n.s.	n.s.	n.s.
Chl *a*	n.s.	<0.0001	n.s.	n.s.	n.s.	n.s.	n.s.
Chl c_2	n.s.	<0.0001	n.s.	n.s.	n.s.	n.s.	n.s.
F_v/F_m	<0.05	<0.0001	0.0001	<0.05	<0.05	<0.05	n.s.
F_v/F_m recovery	n.s.	<0.0001	n.s.	<0.05	n.s.	n.s.	n.s.
P	<0.05	<0.0001	<0.05	n.s.	<0.05	n.s.	n.s.
σ_{PSII}	<0.05	<0.05	<0.05	n.s.	n.s.	n.s.	<0.05
τ_{Qa}	<0.05	<0.0001	n.s.	n.s.	n.s.	n.s.	n.s.
[RCII]	<0.05	<0.0001	<0.05	<0.05	<0.05	<0.05	n.s.
ETR_{max}	n.s.	<0.0001	<0.05	<0.05	n.s.	n.s.	n.s.
I_k	n.s.	<0.0001	<0.05	<0.05	n.s.	n.s.	n.s.
α	<0.05	<0.05	n.s.	n.s.	n.s.	n.s.	n.s.

Table 3. Growth rate (μ), particulate organic carbon (POC) quota and production, as well as cellular chlorophyll *a* (Chl *a*) and chlorophyll c_2 (Chl c_2) concentrations of *Gemingera cryophila* were determined after 2, 8, and 11 weeks of incubation at 6°C and medium light (ML) in conjunction with ambient pCO_2 (400) and high pCO_2 (1000). Please note that after 11 weeks, the 6°C-medium light-1000 was transferred back to 4°C, referred here as the recovered 6°C-ML-1000 treatment. After 4 weeks of incubation at 4°C, the same physiological parameters were also determined for the recovered 6°C-ML-1000 cells. Values represent the mean and standard deviation ($n = 3$).

Treatment	Incubation period	μ (d^{-1})	POC (pg $cell^{-1}$)	POC production (pg $cell^{-1}$ d^{-1})	Chl *a* (pg $cell^{-1}$)	Chl c_2 (pg $cell^{-1}$)
6°C-ML-400	2 weeks	0.19 ± 0.01	121 ± 1	23 ± 1	1.85 ± 0.04	0.17 ± 0.03
6°C-ML-1000	8 weeks	0.03 ± 0.01	231 ± 4	7 ± 2	No data	No data
6°C-ML-1000	11 weeks	0.00 ± 0.00	No data	No data	1.14 ± 0.04	0.15 ± 0.03
Recovered 6°C-ML-1000	4 weeks	0.27 ± 0.01	121 ± 16	33 ± 4	1.78 ± 0.25	0.17 ± 0.02

The cellular POC contents and C/N ratios remained unchanged in all treatments irrespective of the applied environmental factor (Fig. 4B,C). While pCO_2 did not affect the POC production of the cryptophyte, temperature ($p < 0.0001$) and high light ($p < 0.0001$) alone strongly altered POC production (Table 2). There was a significant interaction between temperature and light on POC production of the cryptophyte ($p < 0.05$; Fig. 4D; Table 2), with the lowest POC production rates observed in the two 2°C-high light treatments, whereas values were similar in all other treatments. For the 6°C-medium light-400 treatment, growth continuously decreased and cellular POC quotas were enhanced compared to the 2°C- and 4°C-medium light-400 treatments after just 2 weeks of incubation (Fig. 4B; Table 3). Although POC quota were highest in the 6°C-medium light-1000 treatment at 8-week incubation (Table 3), the latter had the lowest POC production among all treatments (Fig. 4D; Table 3). However, when transferred back to 4°C after 11 weeks of incubation under 6°C-medium light-400 treatment, cells exhibited similar high POC production rates (Table 3) as cells grown at 4°C-medium light-400 (Fig. 4D).

Cellular Chl *a* and Chl c_2 quotas of *G. cryophila* were only influenced by high light alone ($p < 0.0001$; Fig. 4E,F). In response to increasing irradiance ($p < 0.0001$), cellular pigment concentrations were reduced regardless of the applied temperature or pCO_2 level. As for the 6°C-medium light-400 treatment

after 2-week incubation, pigment concentrations were comparable to that of the 2°C and 4°C at medium light (Fig. 4E,F; Table 3). The 6°C-medium light-1000 lowered its Chl *a* concentration after 11 weeks of incubation (1.14 ± 0.04 pg cell^{-1}), but increased its Chl *a* content again (1.78 ± 0.25 pg cell^{-1}) after transferring it back to 4°C (Table 3).

Photophysiology

The dark-adapted maximum quantum yield of PSII (photosynthetic yield, F_v/F_m) was similarly influenced by high pCO_2 temperature and irradiance (Fig. 5A). A significant pCO_2 effect on photosynthetic yield ($p < 0.05$) was observed only in the 2°C-medium light treatment, wherein values increased in response to high pCO_2.

No temperature effect was observed in the yield across all high light treatments, while at medium light increasing temperature (4°C) led to a significant increase in photosynthetic yield ($p < 0.0001$) only under ambient pCO_2, but had no effect under high pCO_2. Hence, there was a significant interaction between temperature and pCO_2 on photosynthetic yield ($p < 0.05$; Fig. 5A). Increasing irradiance had a negative effect on the yield in all treatments ($p < 0.0001$) except for the 2°C-400 treatment, wherein values remained unchanged (Fig. 5A). Cellular concentrations of functional PSII reaction centers ([RCII]) were affected by each environmental factor alone (light: $p < 0.0001$; pCO_2: $p < 0.05$; temperature: $p < 0.05$) as well as their combination in that highest [RCII] was seen in the 2°C-400-medium light treatment (Fig. 5B; Table 2). In response to high pCO_2, [RCII] in the 2°C-medium light treatment was reduced by 33% ($p < 0.05$) while it remained the same in all other treatments. Increasing temperature (up to 4°C) significantly reduced the concentration of reaction centers under medium light-400 while a negative high light effect was observed only in the 2°C-400 treatment (Fig.5B). Different from increasing temperature, high light ($p < 0.0001$) alone significantly influenced the reoxidation times of the primary electron acceptor Qa (τ_{Qa}), with high irradiance significantly reducing τ_{Qa} in both temperature treatments irrespective of pCO_2 level ($p < 0.0001$) (Fig. 5C).

The 6°C-medium light-400 (2-week incubation) exhibited comparable photosynthetic yield, *P*, [RCII], and τ_{Qa} values to that of the 2°C- and 4°C-medium light treatments (Fig. 5; Tables 4). However, the 6°C-medium light-1000 treatment decreased its photosynthetic yield while increasing the number of PSII reaction centers after 11 weeks of incubation. When the latter was transferred back to 4°C, cells fully recovered and shared the same photophysiological characteristics (photosynthetic yield, *P*, σ_{PSII}, τ_{Qa}; Table 4**)** with that of the 4°C-400-medium light treatment (Fig. 5; Supporting Information Table S1).

The different treatments distinctively affected the magnitude and shape of absolute ETRs (Fig. 6A,B). While light ($p < 0.0001$) and temperature ($p < 0.05$) alone and their combination ($p < 0.05$) had a significant effect, pCO_2 had no influence on ETR_{max} (Supporting Information Table S1). Increasing

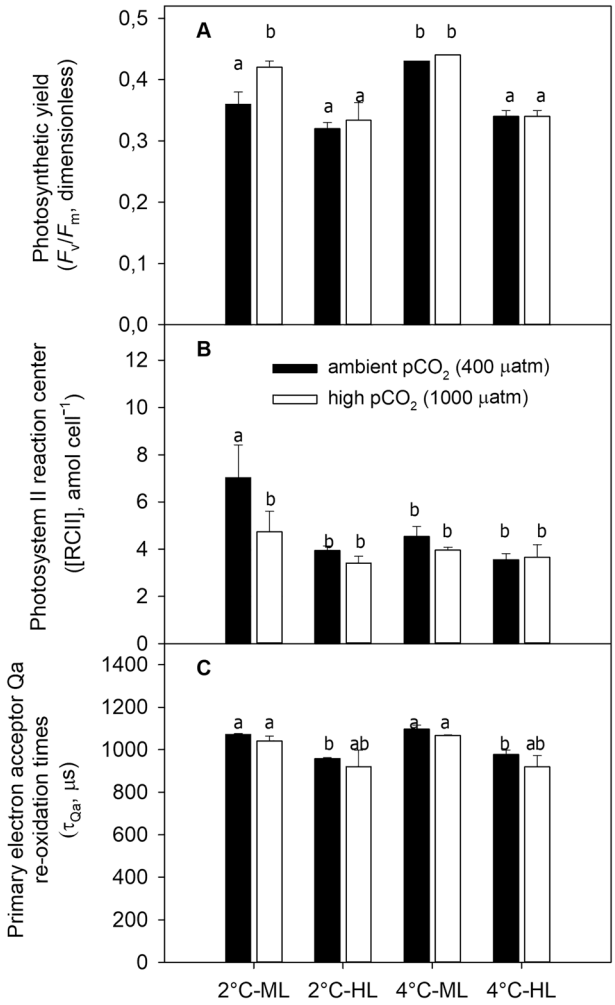

Fig. 5. The dark-adapted maximum photosystem II quantum yield (photosynthetic yield, F_v/F_m) (**A**), cellular concentration of functional PSII reaction centers ([RCII]) (**B**), and reoxidation times of the primary electron acceptor Qa (τ_{Qa}) of *Geminigera cryophila* were determined under ambient pCO_2 (400 μatm, dark bars) and high pCO_2 (1000 μatm, white bars) in combination with different temperature (2°C and 4°C) and light intensity (medium light, ML: 100 μmol photons m^{-2} s^{-1}; high light, HL: 500 μmol photons m^{-2} s^{-1}) treatments at the end of the experiments. Values represent the mean and standard deviation ($n = 3$). Significant differences between the two pCO_2 treatments (post hoc tests) are indicated by varying lower case letters ($p < 0.05$).

temperature decreased ETR_{max} in the high light-400 treatment (Table 4). High light resulted in higher ETR_{max} values relative to medium light irrespective of temperature and pCO_2. ETRs of the 6°C treatments (400 and 1000 pCO_2 at medium light) were significantly reduced (Fig. 6C).

Discussion

The single effect of high pCO_2 on *G. cryophila*

Previous studies have reported no stimulatory effect of high pCO_2-alone on growth of several Antarctic phytoplankton

Table 4. The dark-adapted maximum photosystem II quantum yield (photosynthetic yield, F_v/F_m), energy transfer between photosystem II units (connectivity, *P*), cellular concentration of functional PSII reaction centers ([RCII]), the functional absorption cross-section of PSII (σ_{PSII}), reoxidation times of the primary electron acceptor Q_a (τ), maximum electron transport rates (ETR_{max}), minimum saturating irradiance (I_k), and the maximum light utilization efficiency (α) of *Geminigera cryophila* were determined after 2 and 11 weeks of incubation at 6°C and medium light in conjunction with 400 μatm (400) and 1000 μatm (1000) pCO_2. Please note that after 11 weeks, the 6°C-medium light-1000 treatment was transferred back to 4°C, referred here as the recovered 6°C-medium light-1000 treatment. After 4 weeks of incubation at 4°C, the same photophysiological parameters were also determined for the recovered 6°C-medium light-1000 cells. Values represent the mean and standard deviation ($n = 3$).

Treatment	Incubation period	F_v/F_m (dimensionless)	*P* (dimensionless)	[RCII] (amol cell^{-1})	σ_{PSII} nm^2 PSII^{-1}	τ_{Qa} (μs)	ETR_{max} (e$^-$ PSII^{-1} s^{-1})	I_k (μmol photons m^{-2} s^{-1})	α (rel. unit)
6°C-medium light-400	2 weeks	0.40 ± 0.04	0.40 ± 0.07	6.12 ± 0.38	3.76 ± 0.27	1280 ± 156	56 ± 0	19 ± 5	3.12 ± 0.70
6°C-medium light-1000	11 weeks	0.30 ± 0.04	0.24 ± 0.04	8.57 ± 0.13	3.65 ± 0.38	1049 ± 55	70 ± 5	28 ± 11	2.65 ± 0.75
Recovered 6°C-medium light-1000	4 weeks	0.45 ± 0.01	0.44 ± 0.01	3.45 ± 0.20	4.29 ± 0.18	1065 ± 32	120 ± 26	49 ± 24	2.68 ± 0.67

species, in particular, even negative high pCO_2 effects were found for Antarctic diatoms in conjunction with high irradiance (Trimborn et al. 2013, 2017*a*; Hoppe et al. 2015; Heiden et al. 2016, 2018). Different to diatoms, flagellates such as *Phaeocystis antarctica* (Trimborn et al. 2017*a*,*b*; Koch et al. 2019) and cryptophytes (Domingues et al. 2014; Sommer et al. 2015; Schulz et al. 2017) seem to be tolerant to ocean acidification even in combination with other environmental factors including high irradiance, iron or warming. Our results are in line with this, as we also show here that growth and POC production of *G. cryophila* were not influenced by increasing pCO_2 under any of the applied light levels (Fig. 4A,D). Our observations are consistent with the results from the same *G. cryophila* strain showing either no (20 and 200 μmol photons m^{-2} s^{-1}, respectively; Trimborn et al. 2019) or a modest stimulatory (100 μmol photons m^{-2} s^{-1}; Camoying et al. 2022) high pCO_2 effect in conjunction with low and medium irradiance.

Previous studies have reported the increased susceptibility of temperate phytoplankton (Chen and Gao 2011; Li and Campbell 2013) and several Antarctic diatoms (e.g., Trimborn et al. 2017*b*; Heiden et al. 2018) to photodamage as a result from high pCO_2. In fact, diatoms were found to be prone to PSII photoinactivation in particular under high pCO_2 and high irradiance (Chen and Gao 2011; Li and Campbell 2013; Trimborn et al. 2017*a*) which may be attributed to the decreased PSII D2 protein turnover rate caused by high pCO_2 (Gao et al. 2018). Indeed, in our study, the number of functional PSII was significantly reduced under high pCO_2 and medium light in *G. cryophila* (Fig. 5B), but this was efficiently counteracted by an increased connectivity between photosystems (*P*) (Supporting Information Table S1), thus ensuring a more efficient distribution of photons among PSII preventing thereby photodamage (Fig. 5C). As in Trimborn et al. (2019), our results indicate that *G. cryophila* was not stressed by high pCO_2 at medium light and 2°C as no further photophysiological adjustments were required (Fig. 5; Supporting Information Table S1).

The single effect of high light on *G. cryophila*

In our study, under ambient pCO_2 and 2°C, increasing light intensity (between 100 and 500 μmol photons m^{-2} s^{-1}) led to a significant reduction in growth of the cryptophyte (Fig. 4A). This is consistent with the previously reported sensitivity of the same strain of *G. cryophila* to high irradiance, where under ambient pCO_2, it was even unable to grow at the highest irradiance of 500 μmol photons m^{-2} s^{-1} (Trimborn et al. 2019). As a common photoacclimation response of phytoplankton to increasing irradiance (Kropuenske et al. 2010; Trimborn et al. 2019), the cryptophyte reduced the cellular concentration of the light-harvesting pigments (Fig. 4E,F) and the number of functional PSII reaction centers (Fig. 5B). POC production rates of the cryptophyte were also strongly reduced (Fig. 4D) which could be due to potential oxidative

stress in the cells from high light exposure (Häder et al. 2015). Higher ETR_{max}, minimum saturating irradiance (I_k), as well as lower light utilization efficiency, were found (Supporting Information Table S1), which suggests a saturation of the Calvin cycle and therewith the need for alternative electron cycling to dissipate the excessive light energy. There was also faster reoxidation of the primary electron acceptor Q_a (τ_{Qa}; Fig. 5C), potentially indicating that the cryptophyte depended on additional electron acceptors such as the Mehler reaction, which is a commonly observed photoprotective mechanism of phytoplankton when exposed to high light intensities (Kranz et al. 2010; Roberty et al. 2014). Under stressful conditions such as suboptimal temperatures and high irradiances, phytoplankton were also reported to enhance lipid production (e.g., Dong et al. 2016; Jaussaud et al. 2020) as lipids are good energy sinks, in particular under excess light (Klok et al. 2013). It could be that the excess light energy was used by the cryptophyte for lipid anabolism, which requires large quantities of ATP and NADPH (Jónasdóttir 2019). In fact, we observed the presence of lipid droplets on *G. cryophila* cells at 2°C (Supporting Information Fig. S2A). Apparently, these photoacclimation characteristics ensured that high light-acclimated cells were able to cope well with short-term high light stress as they had higher yield recovery values compared with the cells grown in medium light under ambient pCO_2 and 2°C (Supporting Information Table S1).

Overall, our results are in line with the observation of Trimborn et al. (2019) that growth and carbon fixation of *G. cryophila* are greatly reduced by high light under ambient pCO_2.

The single effect of high temperature on *G. cryophila*

Aside from iron availability, increasing temperature has been reported to strongly affect phytoplankton productivity in the Southern Ocean under ambient pCO_2 (e.g., Rose et al. 2009; Boyd et al. 2015; Spackeen et al. 2018) and was found to stimulate growth of various Antarctic diatoms (Fiala and Oriol 1990), even under low iron concentrations (Hutchins and Boyd 2016; Zhu et al. 2016). Indeed, the increased temperature was beneficial for *G. cryophila* as its growth and photochemical efficiency were enhanced under ambient pCO_2 and medium light (Figs. 4A, 5A), similar to observations in other Antarctic phytoplankton (e.g., Cheah et al. 2013; Andrew et al. 2019). The higher temperature decreased the appearance of lipid droplets on *G. cryophila* cells (Supporting Information Fig. S2B). Lipid droplets are commonly observed for this cryptophyte species (Deane et al. 2002), and the decrease in the lipid content of *G. cryophila* in response to warming may influence its biochemical composition, which in turn could influence the Antarctic marine food web.

Antarctic phytoplankton usually grows under suboptimal temperatures (~ 0–2°C) and have their calculated optimal growth temperature (T_{opt}) at 5.2°C (Coello-Camba and Agustí 2017). In our study, under ambient pCO_2 and medium light, the calculated T_{opt} for *G. cryophila* was 3.8°C (Fig. 2). This temperature is indeed lower than the calculated value for Antarctic phytoplankton in general (Coello-Camba and Agustí 2017) and fits well the observations of Wang and Smith (2021), which reported a T_{opt} of 4°C for another *G. cryophila* strain. Different to *G. cryophila*, the Antarctic haptophyte *P. antarctica* (Zhu et al. 2017; Andrew et al. 2019) and the diatoms *Chaetoceros flexuosus* and *Thalassiosira antarctica* showed enhanced growth in response to increased temperature up to 5°C (Andrew et al. 2019) while the diatom *Pseudo-nitzschia subcurvata* exhibited highest growth at 8°C (Zhu et al. 2017). Moreover, *G. cryophila* had the lowest maximal thermal limit (T_{maxlim}) at 8°C compared to *P. antarctica* and *P. subcurvata*,

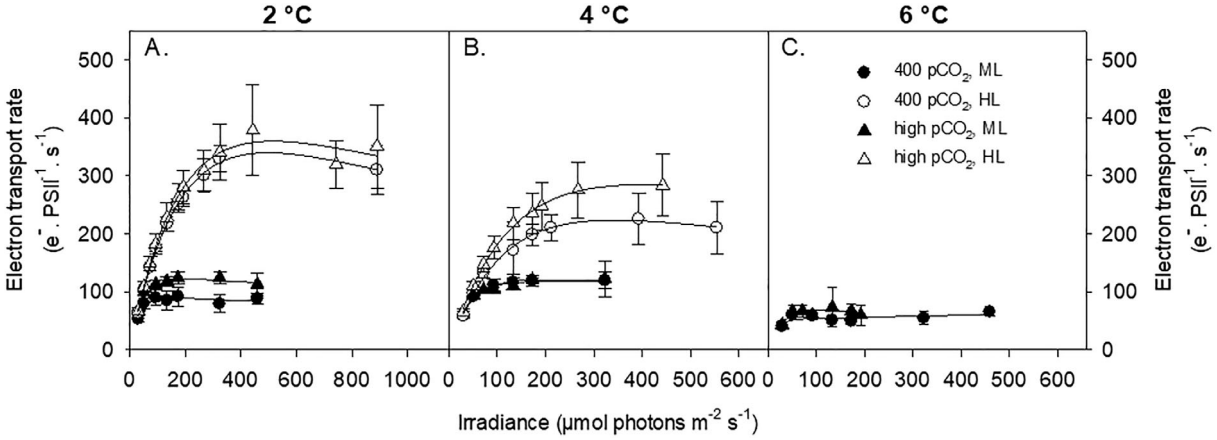

Fig. 6. Absolute electron transport rates were measured in *Geminigera cryophila* grown under ambient pCO_2 (400 μatm, circle) and high pCO_2 (1000 μatm, triangle) in combination with different temperature (2°C (**A**), 4°C (**B**), and 6°C (**C**)) and light intensities (filled symbols, ML, 100 μmol photons m^{-2} s^{-1}; open symbols; HL, 500 μmol photons m^{-2} s^{-1}) at the end of the experiments. Please note that for the 6°C treatment, after 11 weeks of incubation, the unhealthy 6°C-medium light-1000 cells (filled triangle) were transferred back to 4°C to test whether they would be able to recover from exposure to temperature above T_{opt}. Values represent the mean and standard deviation ($n = 3$).

which had their T_{maxlim} at 10°C and 14°C, respectively (Buma et al. 1991; Zhu et al. 2017). Hence, in comparison to other species, the cryptophyte *G. cryophila* had a narrow thermal limit. This indicates that the cryptophyte *G. cryophila* may be less competitive to haptophytes and diatoms under future increased temperatures in the Southern Ocean.

The combined effects of increased temperature, light, and pCO_2

Interestingly, the previously observed negative effects of high light on growth and POC production at 2°C were alleviated at 4°C, as at T_{opt} growth and POC production remained unchanged between medium light and high light under ambient pCO_2 (Fig. 4A,D). This may indicate that at T_{opt}, the generally faster enzymatic reactions might have enabled the cryptophyte to keep up with the high excitation pressure from exposure to high light. Indeed, faster carboxylation rates of RubisCO were previously observed in Antarctic phytoplankton under warming (Young et al. 2015*b*). Increasing temperature in combination with high pCO_2 even promoted the growth of the cryptophyte under high light (Fig. 4A). Under these conditions, to reduce HL stress the cryptophyte rearranged its photophysiological machinery to capture less light. As a consequence, it had less pigments and PSII (Figs. 4E,F, 5B), lowering thereby its light saturation point (Supporting Information Table S1). Still, this did not prevent ETR_{max} to be increased (Supporting Information Table S1). Hence, the excess light energy was potentially drained via additional electron acceptors such as Mehler, as indicated by the faster τ_{Qa} (Fig. 5C). Similar to the temperate cryptophyte *Teleaulax amphioxeia* (Gaillard et al. 2020), *G. cryophila* was mainly influenced by temperature and irradiance and not by high pCO_2. Based on our results, it becomes evident that the previously observed negative effects of high light alone on growth of the cryptophyte were alleviated by warming. This suggests that under future climatic condition, where both warming as well as higher light availability are expected, both environmental factors (warming up to 4°C and light intensities up to 500 μmol photons m^{-2} s^{-1}) together could stimulate growth of *G. cryophila* in the future.

Exposure to 6°C impacts the growth of *G. cryophila*

Temperatures between 6°C and 9°C were reported to be already lethal to several Antarctic diatoms (i.e., *Corethron criophila*, *Nitzschia* spp., *Synedra* sp.) (Fiala and Oriol 1990). Results of our study are in line with this previous finding as we also observed that growth and POC production of *G. cryophila* were severely impacted at 6°C (Fig. 3; Table 3). Compared to the 2°C- and 4°C-medium light-400 treatments, POC quotas of the 6°C-medium light-400 (2-week incubation time; Table 3) were enhanced but this did not lead to increased POC production due to the lowered growth. In fact, ETRs were dramatically reduced under this treatment relative to the 4°C-400-medium light treatment (60 e^- $PSII^{-1}$ s^{-1} [2-week incubation time; Table 4] and 130 e^- $PSII^{-1}$ s^{-1} [Supporting Information Table S1], respectively). After 4 weeks of incubation, the 6°C-medium light-400 already stopped growing, indicating that *G. cryophila* was unable to survive at 6°C under ambient pCO_2. It was only the 6°C-medium light-1000 which was able to somehow sustain a very minimal growth until ca. 10 weeks of incubation (Fig. 3). As for the photophysiological response, the unhealthy cells of the 6°C-medium light-1000 treatment (11 weeks incubation) showed reduced photosynthetic yield, as indicated by the lower F_v/F_m values (0.30 ± 0.04; Table 4) relative to the ones of the 4°C-medium light-1000 treatment (0.44 ± 0.00) (Fig. 5A). This in line with the observation that thermal stress can also cause physical dissociation of the PSII reaction centers and the light-harvesting complex (Armond et al. 1980). In addition, the 6°C-medium light-1000 (11-week incubation) also had the highest concentration of PSII reaction centers (Table 4) among all other experimental treatments (Fig. 5B). As observed in the cyanobacteria *Synechocystis* sp. (Ueno et al. 2016), exposure to temperatures above T_{opt} might have led to more efficient PSII repair in *G. cryophila*, potentially resulting from supposedly enhanced production of the D1 protein, which is a key subunit of PSII. Overall, our results suggest that although growth of the cryptophyte was strongly impacted at 6°C, the high pCO_2-medium light treatment was able to maintain functional reaction centers, enabling it to still fix carbon. But clearly, these results further show that the cells were unable to keep this physiological state as after 11 weeks of incubation at the growth temperature of 6°C, *G. cryophila* did not survive.

In summary, *G. cryophila* was drastically impacted by 6°C warming as growth of this treatment stopped after several weeks of incubation. This indicates the inability of the cryptophyte to tolerate supraoptimal temperatures over a longer period. Interestingly, similar to the observation of Trimborn et al. (2019), high pCO_2 somehow had also a beneficial effect on *G. cryophila* under heat stress exposure as it fully recovered once it was transferred back to 4°C. This may be an important finding given that heat waves are becoming more frequent in the Southern Ocean (González-Herrero et al. 2022).

Implications

Consistent with the results of previous studies (Trimborn et al. 2019; Camoying et al. 2022), the Antarctic cryptophyte *G. cryophila* was not affected by high pCO_2. In line with the observations of Trimborn et al. (2019) at ambient temperature (2°C), exposure to high light irrespective of the applied pCO_2 impacted growth and POC production of *G. cryophila*. As in most Antarctic phytoplankton studied so far (e.g., Rose et al. 2009; Zhu et al. 2017; Andrew et al. 2019), a projected 2°C increase in the Southern Ocean temperature would be beneficial for the growth of *G. cryophila*. In fact, increasing temperature up to 4°C even alleviated the negative effects of

high light on the physiology of the cryptophyte. It is interesting to note that under high pCO_2, the cryptophyte was able to fully recover from heat stress (6°C) after transferring it back to 4°C (T_{opt}). This may indicate that *G. cryophila* may have a competitive advantage when exposed to more frequent heat waves (e.g., González-Herrero et al. 2022). However, on a longer term, in a future warming scenario when grown under temperatures higher than 4°C, *G. cryophila* would, however, be outcompeted by other Antarctic phytoplankton groups such as diatoms due to its narrower thermal limit. Hence, similar to the study of Zhu et al. (2017) on Antarctic diatoms and prymnesiophytes, our results indicate that while pCO_2 may not be a major controlling factor for the distribution of cryptophytes in the Southern Ocean, primarily warming and increasing irradiance will control the growth of *G. cryophila* in the future.

Data availability statement

The data that support the findings of this study will be available at PANGAEA after publication (https://www.pangaea.de).

References

Andrew, S. M., H. T. Morell, R. F. Strzepek, P. W. Boyd, and M. J. Ellwood. 2019. Iron availability influences the tolerance of Southern Ocean phytoplankton to warming and elevated irradiance. Front. Mar. Sci. **6**: 681. doi:10.3389/fmars.2019.00681

Armond, P. A., O. Björkman, and L. A. Staehelin. 1980. Dissociation of supramolecular complexes in chloroplast membranes a manifestation of heat damage to the photosynthetic apparatus. Biochim. Biophys. Acta **601**: 433–442. doi:10.1016/0005-2736(80)90547-7

Boyd, P. W., T. L. Sinikka, D. M. Glover, and S. C. Doney. 2015. Biological ramifications of climate-change-mediated oceanic multi-stressors. Nat. Clim. Change **5**: 71–79. doi:10.1038/nclimate2441

Brown, M. S., D. R. Munro, C. J. Feehan, C. Sweeney, H. W. Ducklow, and O. M. Schofield. 2019. Enhanced oceanic CO_2 uptake along the rapidly changing West Antarctic peninsula. Nat. Clim. Change **9**: 678–683. doi:10.1038/s41558-019-0552-3

Brown, M. S., J. S. Bowman, Y. Lin, C. J. Feehan, C. M. Moreno, N. Cassar, A. Marchetti, and O. M. Schofield. 2021. Low diversity of a key phytoplankton group along the West Antarctic peninsula. Limnol. Oceanogr. **66**: 2470–2480. doi:10.1002/lno.11765

Buma, A. G. J., N. Bano, M. J. W. Veldhuis, and G. W. Kraay. 1991. Comparison of the pigmentation of two strains of the prymnesiophyte *Phaeocystis* sp. Neth. J. Sea Res. **27**: 173–182. doi:10.1016/0077-7579(91)90010-X

Camoying, M. G., K. Bischof, J. K. Geuer, B. P. Koch, and S. Trimborn. 2022. In contrast to diatoms, cryptophytes are susceptible to iron limitation, but not to ocean acidification. Physiol. Plant. **174**: e13614. doi:10.1111/ppl.13614

Cheah, W., A. McMinn, F. B. Griffiths, K. J. Westwood, S. W. Wright, and L. A. Clementson. 2013. Response of phytoplankton photophysiology to varying environmental conditions in the sub-Antarctic and polar frontal zone. PLoS One **8**: e72165. doi:10.1371/journal.pone.0072165

Chen, S., and K. S. Gao. 2011. Solar ultraviolet radiation and CO_2-induced ocean acidification interacts to influence the photosynthetic performance of the red tide alga *Phaeocystis globosa* (Prymnesiophyceae). Hydrobiologia **675**: 105–117. doi:10.1007/s10750-011-0807-0

Coello-Camba, A., and S. Agustí. 2017. Thermal thresholds of phytoplankton growth in polar waters and their consequences for a warming polar ocean. Front. Mar. Sci. **4**: 168. doi:10.3389/fmars.2017.00168

Deane, J. A., I. M. Strachan, G. W. Saunders, D. R. A. Hill, and G. I. McFadden. 2002. Cryptomonad evolution: Nuclear 18S rDNA phylogeny versus cell morphology and pigmentation. J. Phycol. **38**: 1236–1244. doi:10.1046/j.1529-8817.2002.01250.x

Dickson, A. G., and F. J. Millero. 1987. A comparison of the equilibrium constants for the dissociation of carbonic acid in seawater media. Deep-Sea Res. A: Oceanogr. Res. Pap. **34**: 1733–1743. doi:10.1016/0198-0149(87)90021-5

Domingues, R. B., C. C. Guerra, A. B. Barbosa, V. Brotas, H. M. Galvao, and A. Notes. 2014. Effects of ultraviolet radiation and CO_2 increase on winter phytoplankton assemblages in a temperate coastal lagoon. J. Plankton Res. **36**: 672–684. doi:10.1093/plankt/fbt135

Donahue, K., C. Klaas, P. W. Dillingham, and L. J. Hoffmann. 2019. Combined effects of ocean acidification and increased light intensity on natural phytoplankton communities from two Southern Ocean water masses. J. Plankton Res. **41**: 30–45. doi:10.1093/plankt/fby048

Dong, H. P., Y. L. Dong, L. Cui, S. Balamurugan, J. Gao, S. H. Lu, and T. Jiang. 2016. High light stress triggers distinct proteomic responses in the marine diatom *Thalassiosira pseudonana*. BMC Genomics **17**: 994. doi:10.1186/s12864-016-3335-5

Fiala, M., and L. Oriol. 1990. Light-temperature interactions on the growth of Antarctic diatoms. Polar Biol. **10**: 629–636. doi:10.1007/BF00239374

Frölicher, T. L., J. L. Sarmiento, D. J. Paynter, J. P. Dunne, J. P. Krasting, and M. Winton. 2015. Dominance of the Southern Ocean in anthropogenic carbon and heat uptake in CMIP5 models. J. Climate **28**: 862–886. doi:10.1175/JCLI-D-14-00117.1

Gaillard, S., and others. 2020. Combined effects of temperature, irradiance, and pH on *Teleaulax amphioxeia* (Cryptophyceae) physiology and feeding ratio for its predator *Mesodinium rubrum* (Ciliophora). J. Phycol. **56**: 775–783. doi:10.1111/jpy.12977

Gao, G., Z. Xu, Q. Shi, and H. Wu. 2018. Increased CO_2 exacerbates the stress of ultraviolet radiation on photosystem II function in the diatom *Thalassiosira weissflogii*. Environ. Exp. Bot. **156**: 96–105. doi:10.1016/j.envexpbot.2018.08.031

Genty, B., J. M. Briantais, and N. R. Baker. 1989. The relationship between the quantum yield of photosynthetic electron transport and quenching of chlorophyll fluorescence. Biochim. Biophys. Acta **990**: 87–92. doi:10.1016/S0304-4165(89)80016-9

González-Herrero, S., D. Barriopedro, R. M. Trigo, J. López-Bustins, and M. Oliva. 2022. Climate warming amplified the 2020 record-breaking heatwave in the Antarctic Peninsula. Commun. Earth Environ. **3**: 122. doi:10.1038/s43247-022-00450-5

Guillard, R. R., and J. H. Ryther. 1962. Studies of marine planktonic diatoms. 1. *Cyclotella nana* (Hustedt) and *Detonula confervacea* (Cleve) gran. Can. J. Microbiol. **8**: 229–239. doi:10.1139/m62-029

Häder, D. P., and others. 2015. Effects of UV radiation on aquatic ecosystems and interactions with other environmental factors. Photochem. Photobiol. Sci. **14**: 108–126. doi:10.1039/c4pp90035a

Heiden, J. P., K. Bischof, and S. Trimborn. 2016. Light intensity modulates the response of two Antarctic diatom species to ocean acidification. Front. Mar. Sci. **3**: 260. doi:10.3389/fmars.2016.00260

Heiden, J. P., S. Thoms, K. Bischof, and S. Trimborn. 2018. Ocean acidification stimulates particulate organic carbon accumulation in two Antarctic diatom species under moderate and high solar radiation. J. Phycol. **54**: 505–517. doi:10.1111/jpy.12753

Heiden, J. P., and others. 2019. Impact of ocean acidification and high solar radiation on productivity and species composition of a late summer phytoplankton community of the coastal Western Antarctic Peninsula. Limnol. Oceanogr. **64**: 1716–1736. doi:10.1002/lno.11147

Hoegh-Guldberg, O., and J. F. Bruno. 2010. The impact of climate change on the world's marine ecosystem. Science **328**: 1523–1528. doi:10.1126/science.118993

Hoppe, C. J. M., L. Holtz, S. Trimborn, and B. Rost. 2015. Ocean acidification decreases the light-use efficiency in an Antarctic diatom under dynamic but not constant light. New Phytol. **207**: 159–171. doi:10.1111/nph.13334

Hutchins, D. A., and P. W. Boyd. 2016. Marine phytoplankton and the changing ocean iron cycle. Nat. Clim. Change **6**: 1072–1079. doi:10.1038/nclimate3147

IPCC. 2014. *In* R. K. Pachauri and L. A. Meyer [eds.], Climate change 2014: Synthesis report. Contribution of working groups I, II and III to the fifth assessment report of the intergovernmental panel on climate change. IPCC.

IPCC. 2019. *In* H.-O. Pörtner and others [eds.], IPCC special report on the ocean and cryosphere in a changing climate. IPCC.

Jaussaud, A., J. Lupette, J. Salvaing, J. Jouhet, O. Bastien, M. Gromova, and E. Maréchal. 2020. Stepwise biogenesis of subpopulations of lipid droplets in nitrogen starved *Phaeodactylum tricornutum* cells. Front. Plant Sci. **11**: 48. doi:10.3389/fpls.2020.00048

Jónasdóttir, S. H. 2019. Fatty acid profiles and production in marine phytoplankton. Mar. Drugs **17**: 151. doi:10.3390/md17030151

Jones, M. E., D. H. Bromwich, J. P. Nicolas, J. Carrasco, E. Plavcová, X. Zou, and S.-H. Wang. 2019. Sixty years of widespread warming in the southern middle and high latitudes (1957–2016). J. Climate **32**: 6875–6898. doi:10.1175/JCLI-D-18-0565.1

Klok, A. J., D. E. Martens, R. H. Wijffels, and P. P. Lamers. 2013. Simultaneous growth and neutral lipid accumulation in microalgae. Bioresour. Technol. **134**: 233–243. doi:10.1016/j.biortech.2013.02.006

Koch, F., S. Beszteri, L. Harms, and S. Trimborn. 2019. The impacts of iron limitation and ocean acidification on the cellular stoichiometry, photophysiology and transcriptome of *Phaeocystis antarctica*. Limnol. Oceanogr. **64**: 357–375. doi:10.1002/lno.11045

Kolber, Z. S., O. Prášil, and P. G. Falkowski. 1998. Measurements of variable chlorophyll fluorescence using fast repetition rate techniques: Defining methodology and experimental protocols. Biochim. Biophys. Acta **1367**: 88–106. doi:10.1016/S0005-2728(98)00135-2

Kranz, S. A., O. Levitan, K. Richter, O. Prasil, I. Berman-Frank, and B. Rost. 2010. Combined effects of CO_2 and light on the N_2-fixing cyanobacterium *Trichodesmium* IMS101: Physiological responses. Plant Physiol. **154**: 334–345. doi:10.1104/pp.110.159145

Kropuenske, L. R., M. M. Mills, G. L. van Dijken, A. C. Alderkamp, G. Mine Berg, D. H. Robinson, N. A. Welschmeyer, and K. R. Arrigo. 2010. Strategies and rates of photoacclimation in two major Southern Ocean phytoplankton taxa: *Phaeocystis antarctica* (Haptophyta) and *Fragilariopsis cylindrus* (Bacillariophyceae). J. Phycol. **46**: 1138–1151. doi:10.1111/j.1529-8817.2010.00922.x

Li, G., and D. A. Campbell. 2013. Rising CO_2 interacts with growth light and growth rate to alter photosystem II photoinactivation of the coastal diatom *Thalassiosira pseudonana*. PLoS One **8**: e55562. doi:10.1371/journal.pone.0055562

Mehrbach, C., C. Culberson, J. Hawley, and R. Pytkowicx. 1973. Measurements of the apparent dissociation constants of carbonic acid in seawater at atmospheric pressure. Limnol. Oceanogr. **18**: 897–907. doi:10.4319/lo.1973.18.6.0897

Mendes, C. R. B., V. M. Tavano, M. C. Leal, M. S. de Souza, V. Brotas, and C. A. E. Garcia. 2013. Shifts in the dominance between diatoms and cryptophytes during three late summers in the Bransfield Strait (Antarctic peninsula). Polar Biol. **36**: 537–547. doi:10.1007/s00300-012-1282-4

Meyer, M. A., and S. Z. El-Sayed. 1983. Grazing of *Euphausia superba* Dana on natural phytoplankton populations. Polar Biol. **1**: 193–197. doi:10.1007/BF00443187

Moore, J. K., and others. 2018. Sustained climate warming drives declining marine biological productivity. Science **359**: 1139–1143. doi:10.1126/science.aao6379

Pierrot, D., E. Lewis, and D. Wallace. 2006. MS excel program developed for CO_2 system calculations. ORNL/CDIAC-105. U.S. Department of Energy.

Ralph, P. J., and R. Gademann. 2005. Rapid light curves: A powerful tool to assess photosynthetic activity. Aquat. Bot. **82**: 222–237. doi:10.1016/j.aquabot.2005.02.006

Ratkowsky, D. A., R. K. Lowry, T. A. McMeekin, A. N. Stokes, and R. E. Chandler. 1983. Model for bacterial culture growth rate throughout the entire biokinetic temperature range. J. Bacteriol. **154**: 1222–1226. doi:10.1128/jb.154.3.1222-1226.1983

Redfield, A. C. 1958. The biological control of chemical factors in the environment. Am. Sci. **64**: 205–221.

Roberty, S., B. Bailleul, N. Berne, F. Franck, and P. Cardol. 2014. PSI Mehler reaction is the main alternative photosynthetic electron pathway in *Symbiodinium* sp., symbiotic dinoflagellates of cnidarians. New Phytol. **204**: 81–91. doi:10.1111/nph.12903

Rose, J. M., and others. 2009. Synergistic effects of iron and temperature on Antarctic phytoplankton and microzooplankton assemblages. Biogeosciences **6**: 3131–3147. doi:10.5194/bg-6-3131-2009

Schofield, O., G. Saba, K. Coleman, F. Carvalho, N. Couto, and H. Ducklow. 2017. Decadal variability in coastal phytoplankton community composition in a changing West Antarctic Peninsula. Deep-Sea Res. I: Oceanogr. Res. Pap. **124**: 42–54. doi:10.1016/j.dsr.2017.04.014

Schulz, K. G., and others. 2017. Phytoplankton blooms at increasing levels of atmospheric carbon dioxide: Experimental evidence for negative effects on prymnesiophytes and positive on small picoeukaryotes. Front. Mar. Sci. **4**: 64. doi:10.3389/fmars.2017.00064

Sommer, U., C. Paul, and M. Moustaka-Gouni. 2015. Warming and ocean acidification effects on phytoplankton—From species shifts to size shifts within species in a mesocosm experiment. PLoS One **10**: e0125239. doi:10.1371/journal.pone.0125239

Spackeen, J. L., and others. 2018. Impact of temperature, CO_2, and iron on nutrient uptake by a late-season microbial community from the Ross Sea, Antarctica. Aquat. Microb. Ecol. **82**: 145–159. doi:10.3354/ame01886

Suggett, D. J., H. L. MacIntyre, and R. J. Geider. 2004. Evaluation of biophysical and optical determinations of light absorption by photosystem II in phytoplankton. Limnol. Oceanogr.: Methods **2**: 316–332. doi:10.4319/lom.2004.2.316

Suggett, D. J., C. M. Moore, A. E. Hickman, and R. J. Geider. 2009. Interpretation of fast repetition rate (FRR) fluorescence: Signatures of phytoplankton community structure versus physiological state. Mar. Ecol. Prog. Ser. **376**: 1–19. doi:10.3354/meps07830

Trimborn, S., T. Brenneis, E. Sweet, and B. Rost. 2013. Sensitivity of Antarctic phytoplankton species to ocean acidification: Growth, carbon acquisition and species interaction. Limnol. Oceanogr. **58**: 997–1007. doi:10.4319/lo.2013.58.3.0997

Trimborn, S., S. Thoms, T. Brenneis, J. P. Heiden, S. Beszteri, and K. Bischof. 2017*a*. Two Southern Ocean diatoms are more sensitive to ocean acidification and changes in irradiance than the prymnesiophyte *Phaeocystis antarctica*. Physiol. Plant. **160**: 155–170. doi:10.1111/ppl.12539

Trimborn, S., T. Brenneis, C. J. M. Hoppe, L. Norman, J. Santos, L. Laglera, D. Wolf-Gladrow, and C. Hassler. 2017*b*. Iron sources alter the response of Southern Ocean phytoplankton to ocean acidification. Mar. Ecol. Prog. Ser. **578**: 35–50. doi:10.3354/meps12250

Trimborn, S., S. Thoms, P. Karitter, and K. Bischof. 2019. Ocean acidification and high irradiance stimulate the photo-physiological fitness, growth and carbon production of the Antarctic cryptophyte *Geminigera cryophila*. Biogeosciences **16**: 2997–3008. doi:10.5194/bg-16-2997-2019

Ueno, M., P. Sae-Tang, Y. Kusama, Y. Hihara, M. Matsuda, T. Hasunuma, and Y. Nishiyama. 2016. Moderate heat stress stimulates repair of photosystem II during photoinhibition in *Synechocystis* sp. PCC 6803. Plant Cell Physiol. **57**: 2417–2426. doi:10.1093/pcp/pcw153

Wang, X., and W. O. Smith. 2021. Phytoplankton growth at low temperatures: Results from low temperature incubations. J. Plankton Res. **43**: 633–641. doi:10.1093/plankt/fbab054

Weisse, T., and P. Stadler. 2006. Effect of pH on growth, cell volume, and production of freshwater ciliates, and implications for their distribution. Limnol. Oceanogr. **51**: 1708–1715. doi:10.4319/lo.2006.51.4.1708

Young, J. N., S. A. Kranz, J. A. L. Goldman, P. D. Tortell, and F. M. M. Morel. 2015*a*. Antarctic phytoplankton downregulate their carbon-concentrating mechanisms under high CO_2 with no change in growth rates. Mar. Ecol. Progr. Ser. **532**: 13–28. doi:10.3354/meps11336

Young, J. N., J. A. L. Goldman, S. A. Kranz, P. D. Tortell, and F. M. M. Morel. 2015*b*. Slow carboxylation of rubisco constrains the rate of carbon fixation during Antarctic phytoplankton blooms. New Phytol. **205**: 172–181. doi:10.1111/nph.13021

Zhu, Z., K. Xu, F. Fu, J. L. Spackeen, D. A. Bronk, and D. A. Hutchins. 2016. A comparative study of iron and temperature interactive effects on diatoms and *Phaeocystis antarctica* from the Ross Sea, Antarctica. Mar. Ecol. Prog. Ser. **550**: 39–51. doi:10.3354/meps11732

Zhu, Z., P. Qu, J. Gale, F. Fu, and D. A. Hutchins. 2017. Individual and interactive effects of warming and CO_2 on *Pseudo-nitzschia subcurvata* and *Phaeocystis Antarctica*, two dominant

phytoplankton from the Ross Sea, Antarctica. Biogeosciences **14**: 5281–5295. doi:10.5194/bg-14-5281-2017

Zwietering, M. H., J. T. de Koos, B. E. Hasenack, J. C. de Wit, and K. van't Riet. 1991. Modeling of bacterial growth as a function of temperature. Appl. Environ. Microbiol. **57**: 1094–1101. doi:10.1128/aem.57.4.1094-1101.1991

Acknowledgments

We thank B. Meier-Schlosser and Kai Bischof for pigment analysis, S. Murawski for POC analysis, and A. Cayetano for his help in the data analysis using Python. We are grateful to A. Kraberg for her technical assistance in scanning electron microscopy observations, and S. Rokitta for the insightful discussions on the thermal functional response of phytoplankton. We also thank the members of the EcoTrace Group and the Marine Biogeosciences Section (especially L. Rehder) at the AWI for the diverse logistical support. M. Camoying was supported by the Katholischer Akademischer Ausländerdienst (KAAD) through a PhD fellowship. Open Access funding enabled and organized by Projekt DEAL.

Conflict of Interest

None declared.

Submitted 29 July 2022
Revised 27 February 2023
Accepted 15 June 2023

Associate editor: Bingzhang Chen